

RSC Advances



This article can be cited before page numbers have been issued, to do this please use: M. Das, B. N. Ghosh, A. Bauza, K. Rissanen, A. Frontera and S. Chattopadhyay, *RSC Adv.*, 2015, DOI: 10.1039/C5RA13960K.



This is an *Accepted Manuscript*, which has been through the Royal Society of Chemistry peer review process and has been accepted for publication.

Accepted Manuscripts are published online shortly after acceptance, before technical editing, formatting and proof reading. Using this free service, authors can make their results available to the community, in citable form, before we publish the edited article. This *Accepted Manuscript* will be replaced by the edited, formatted and paginated article as soon as this is available.

You can find more information about *Accepted Manuscripts* in the [Information for Authors](#).

Please note that technical editing may introduce minor changes to the text and/or graphics, which may alter content. The journal's standard [Terms & Conditions](#) and the [Ethical guidelines](#) still apply. In no event shall the Royal Society of Chemistry be held responsible for any errors or omissions in this *Accepted Manuscript* or any consequences arising from the use of any information it contains.

Observation of novel oxygen···oxygen interaction in supramolecular assembly of cobalt(III) Schiff base complexes: A combined experimental and computational study

Mithun Das^a, Biswa Nath Ghosh^b, Antonio Bauzá^c, Kari Rissanen^b, Antonio Frontera^{c,*} and Shouvik Chattopadhyay^{a,*}

^a Department of Chemistry, Inorganic Section, Jadavpur University, Kolkata 700032, India.

^b Department of Chemistry, Nanoscience Center, University of Jyväskylä, P.O. Box 35, 40014 Jyväskylä, Finland.

^c Departament de Química, Universitat de les Illes Balears, Crta. de Valldemossa km 7.5, 07122 Palma de Mallorca (Balears), Spain. E-mail: toni.frontera@uib.es

E-mail: shouvik.chem@gmail.com Tel: +91-33-24572941

Abstract

Two mononuclear cobalt(III) Schiff base complexes with azide [Co(L)(N₃)(L')] (**1**) and [Co(L)(N₃)(L'')] (**2**) {where HL = 1-((2-(diethylamino)ethylimino)methyl)naphthalene-2-ol, HL' = 2-hydroxy-1-naphthaldehyde and HL'' = acetylacetone} have been synthesized and characterized by elemental analysis, IR and UV–Vis spectroscopy and single crystal X-ray diffraction studies. Both complexes show mononuclear structures with azide as terminal coligand. Structural features have been examined in detail that reveal the formation of interesting supramolecular networks generated through non-covalent forces including hydrogen bonding, C–

H...H-C and C-H/ π interactions. These interactions have been studied energetically by means of theoretical DFT calculations. We have also analyzed the unexpected O...O interactions observed in one complex between the oxygen atoms of the coordinated aldehyde groups using several computational tools, including Bader's "atoms-in-molecules" (AIM) and natural bond orbital (NBO) analyses.

Keywords: Schiff base; Cobalt(III); Azide; O...O interactions; Theoretical study.

Introduction

Synthesis and structural characterization of transition metal complexes with Schiff base ligands have attracted much attention for their fascinating structures, interesting properties and a variety of appealing applications.¹ Encouragement for their syntheses and characterization is provided by their potential abilities in biological modeling application, e.g. to mimic the active sites of many enzymes.² Focusing to cobalt(III) Schiff base complexes, there is extensive attention in the domain of metallo-organic and coordination chemistry due to their synthetic accessibility, fascinating structural features and diverse range of applications covering organic synthesis, photochemistry,³ magnetic and electrochromism,⁴ and catalysis.⁵ They also have important biological applications.⁶ Recently, dinuclear and mononuclear cobalt(III) Schiff base complexes have also been used as precursor for the synthesis of Co₃O₄ nanoparticles via thermal decomposition method.⁷ Synthesis of Co₃O₄ nanoparticles via thermal decomposition cobalt(III) Schiff base complexes have also been reported in literature.⁷

On the other hand, the formation of supramolecular assemblies is an appealing research topic now-a-days. The most commonly used approach is to employ hydrogen bonds for engineering the structures of such complexes.⁸ The crystalline architecture of the complexes could also be managed by several other well established non-covalent interactions, such as, π -

stacking, cation- π , and C-H/ π forces, which have also attracted considerable interest due to their relative strength, directionality, and ability to act synergically, thereby providing an organizing force for the association of molecules into distinct supramolecular assemblies.⁹ Moreover, other less recognized forces, such as, σ/π -hole, lone-pair/ π and anion/ π interactions, have also been utilized in sensors, probes, photonic devices, catalysis etc.¹⁰ In this context, it is not irrelevant to state that intra-molecular non-bonded interaction between sulfur and sulfur (or oxygen or nitrogen) atoms has also been observed in a large number of organosulfur complexes controlling the conformation of small and large molecules.¹¹ In these molecules, the non-bonded S...S, S...O or S...N distances are significantly shorter than the sum of the corresponding van der Waals radii (3.62, 3.32 or 3.35 Å) in the crystalline structure.¹²

In the present work, we have synthesized two new cobalt(III) azide complexes with a tridentate N₂O donor Schiff base and 2-hydroxynaphthyl-1-carboxaldehyde or acetylacetonate. The structures have been confirmed by single crystal X-ray diffraction analysis. Structural features have been examined in detail that reveal the formation of interesting supramolecular networks generated through non-covalent forces including hydrogen bonding, C-H...H-C and C-H/ π interactions.¹³ These interactions have been studied energetically by means of theoretical DFT calculations.¹⁴ Most interesting observation is the existence of O...O interactions in the supramolecular assembly of one complex. The O...O interactions between the oxygen atoms of the coordinated aldehyde groups have also been analyzed using several computational tools, including Bader's "atoms-in-molecules" (AIM)¹⁵ and natural bond orbital (NBO)¹⁶ analyses.

Experimental Section

Materials and Measurements

All chemicals were of reagent grade and purchased from Sigma-Aldrich. They were used without further purification. **Caution!!!** Since the azide complexes of metal ions are potentially explosive, only small amounts of the materials should be handled with care.

Elemental analysis was performed using a PerkinElmer 240C elemental analyzer. IR spectra in KBr (4500–500 cm^{-1}) were recorded using a PerkinElmer Spectrum Two FT-IR spectrophotometer. ^1H NMR spectrum was recorded on Bruker DRX-300 NMR Spectrometer at 300 MHz using DMSO-d_6 as solvent. Electronic spectra in DMSO (800–300 nm) were recorded in PerkinElmer LAMBDA 35 UV/Vis spectrophotometer. Fluorescence spectra were obtained on SHIMADZU RF-5301PC Spectrofluorophotometer at room temperature. Lifetime measurements were recorded using Hamamatsu MCP photomultiplier (R3809) and were analyzed by using IBHDAS6 software. Intensity decay profiles were fitted to the sum of exponentials series

$$I(t) = \sum_i A_i \exp(-t/\tau_i)$$

where A_i is a factor representing the fractional contribution to the time resolved decay of the component with a lifetime of τ_i . The intensity averaged life times (τ_{av}) are determined using the following equation:

$$\langle \tau \rangle = \frac{\sum_i A_i \tau_i^2}{\sum_i A_i \tau_i}$$

Preparation of ligand HL (1-((2-(diethylamino)ethylimino)methyl)naphthalen-2-ol)

The tridentate Schiff base ligand, HL, was synthesized by refluxing N,N-diethyl-1,2-diaminoethane (1 mmol, 0.14 mL) with 2-hydroxynaphthyl-1-carboxaldehyde, (HL'), (1 mmol, 172 mg) in methanol solution (20 mL) for ca. 30 minutes following literature method.¹⁷ The ligand was not isolated. The methanol solution was used for the syntheses of the complexes.

Preparation of complex [Co(L)(N₃)(L')] (1)

A methanol solution (15 mL) of 2-hydroxynaphthyl-1-carboxaldehyde, (HL'), (1 mmol, 172 mg) and cobalt(II) acetate tetrahydrate (1 mmol, 250 mg) was stirred for ca. 30 minutes. The methanol solution (20 mL) of Schiff base ligand, HL, was then added followed by aqueous solution (5 mL) of sodium azide in stirring condition. The resulting solution was stirred for additional 1 hr and then kept aside in room temperature. Solid product started to separate on standing overnight. Suitable single crystal of **1** for X-ray diffraction was obtained from the acetonitrile solution.

Yield: 340 mg (63%). Anal. Calc. for C₂₈H₂₈CoN₅O₃ (541.48): C, 62.11; H, 5.21; N, 12.93%. Found: C, 62.3; H, 5.3; N, 12.7%. FT-IR (KBr, cm⁻¹): 1618, 1602 (C=O), 1583 (C=N), 2023 (N₃). UV-Vis, λ_{max} (nm) [ε_{max}(L mol⁻¹ cm⁻¹)](Acetonitrile): 219 (90235), 268 (62163) 319 (24645), 404 (6446), 422 (6076). ¹H NMR (DMSO-d₆) (ppm) δ: 9.77 (s, 1H, -CH=O), 8.83 (s, 1H, -CH=N), 8.71 (d, J = 4.18 Hz, 1H, Ar-H), 8.37 (d, J = 4.11 Hz, 1H, Ar-H), 7.60 (m, 3H, Ar-H), 7.45 (m, 3H, Ar-H), 7.28 (dd, J = 7.34, 7.22 Hz, 1H, Ar-H), 7.15 (dd, J = 7.61, 7.53 Hz, 1H, Ar-H), 6.87 (dd, J = 9.07 Hz, 9.09 Hz, 1H, Ar-H), 6.68 (d, J = 9.05 Hz, 1H, Ar-H), 4.38 (m, 2H, -CH₂CH₃), 3.15 (m, 1H, -CH₂CH₂), 2.79 (m, 2H, -CH₂CH₃), 2.06 (m, 2H, -CH₂CH₂), 1.21 (m, 1H, -CH₂CH₂), 1.55 (t, 6.19 Hz, 3H, -CH₂CH₃), 0.76 (t, 6.14 Hz, 3H, -CH₂CH₃).

Preparation of complex [Co(L)(N₃)(L'')] (2)

It was prepared in a similar method to that of **1** except that acetylacetone, (HL''), (1 mmol, 0.1 mL) was used instead of 2-hydroxynaphthyl-1-carboxaldehyde (HL'). Solid product separated on standing overnight. Single crystal suitable for X-ray diffraction was obtained from the acetonitrile solution.

Yield: 290 mg (62%). Anal. Calc. for $C_{22}H_{28}CoN_5O_3$ (469.42): C, 59.41; H, 5.58; N, 13.86%. Found: C, 59.6; H, 5.4; N, 13.7%. FT-IR (KBr, cm^{-1}): 1621 (C=O), 1577 (C=N), 2023 (N_3). UV-Vis, λ_{max} (nm) [$\epsilon_{max}(L mol^{-1} cm^{-1})$](Acetonitrile): 224 (58391), 266 (57462), 408 (5601), 424 (5455). 1H NMR (DMSO- d_6) (ppm) δ : 8.72 (s, 1H, -CH=N), 8.14 (d, $J = 4.26$ Hz, 1H, Ar-H), 7.65 (d, $J = 3.97$ Hz, 1H, Ar-H), 7.55 (d, $J = 4.55$ Hz, 1H, Ar-H), 7.44 (dd, $J = 7.14$, 7.56 Hz, 1H, Ar-H), 7.16 (dd, $J = 7.65$, 7.46 Hz, 1H, Ar-H), 7.08 (d, $J = 4.57$ Hz, 1H, Ar-H), 5.62 (s, 1H, -COCH-), 4.29 (m, 2H, -CH₂CH₃), 3.15 (m, 1H, -CH₂CH₂), 2.91 (m, 1H, -CH₂CH₂), 2.68 (m, 2H, -CH₂CH₃), 2.37 (m, 1H, -CH₂CH₂), 2.27 (s, 3H, -COCH₃), 1.85 (m, 1H, -CH₂CH₂), 1.63 (s, 3H, -COCH₃), 1.06 (t, 6.77 Hz, 3H, -CH₂CH₃), 0.81 (t, 6.99 Hz, 3H, -CH₂CH₃).

X-ray Crystallography

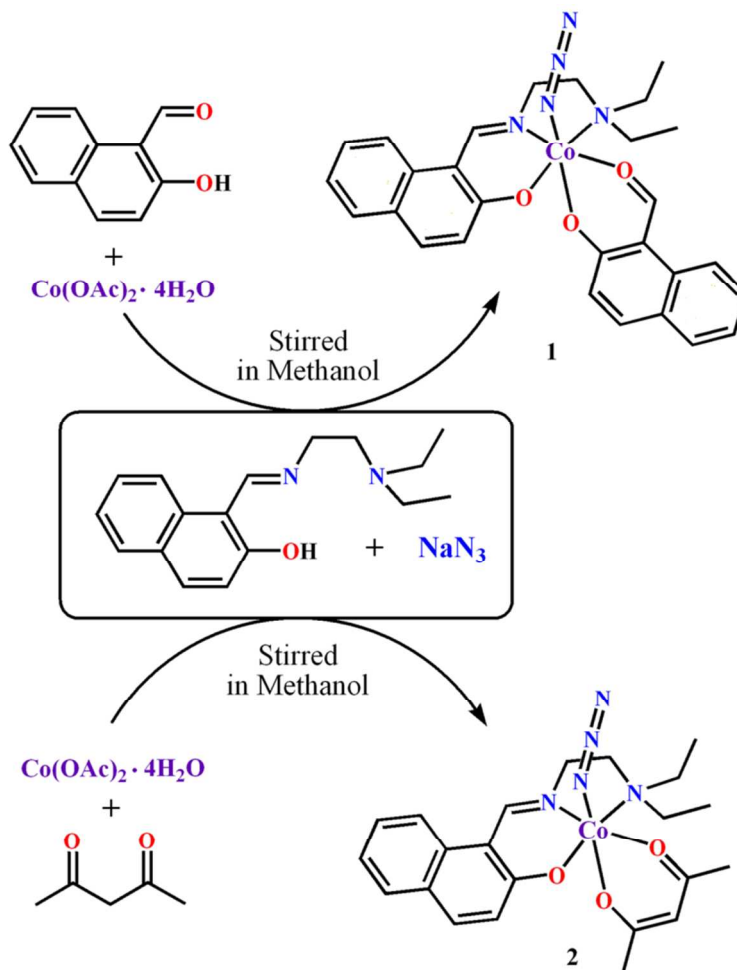
The structural analysis of **1** was performed using Bruker-Nonius Kappa CCD diffractometer equipped with APEX II detector with graphite-monochromatized Mo- $K\alpha$ ($\lambda = 0.71073 \text{ \AA}$) radiation at 123 K. Collect software was used for the data measurement.¹⁸ and DENZO-SMN for the processing.¹⁹ Absorption correction was applied using the multi-scan SADABS programme.²⁰ The unit cell of **1** includes a disordered acetonitrile molecule, which could not be modeled as discrete atomic sites. So the structure was subjected to the SQUEEZE procedure from the PLATON suite to calculate the diffraction contribution of the solvent molecules and there by produce a set of solvent-free diffraction intensities. A void volume of 129 \AA^3 contained a minimum of 16 electrons. Prior to SQUEEZE, all non-hydrogen atoms were made anisotropic and all hydrogen atoms were inserted at their calculated positions. Details of the SQUEEZE procedure are given in the CIF file. Data for **2** were collected at 123 K on an

Agilent Super Nova Dual diffractometer with Atlas detector using mirror-monochromatized Mo- $K\alpha$ ($\lambda = 0.71073 \text{ \AA}$) radiation. CrysAlis Program was used for the data collection and processing.²¹ The intensities were corrected for absorption using the Analytical face index absorption correction method.²² The structures were solved by charge flipping method with SUPERFLIP²³ and refined by full-matrix least-squares methods using the WinGX software,²⁴ which utilizes the SHELXL-97 module.²⁵ All non-hydrogen atoms were refined with anisotropic thermal parameters. Hydrogen atoms were introduced in calculated positions with isotropic thermal parameters using the ‘riding model’. Selected crystallographic data and experimental details of complexes **1** and **2** are summarized in Table 1. CCDC 1047381 (for **1**) and 1047382 (for **2**).

Theoretical Methods

The geometries of the complexes included in this study were computed at the BP86-D3/def2-TZVP level of theory using the crystallographic coordinates within the TURBOMOLE 7.0 program.²⁶ This level of theory that includes the latest available dispersion correction (D3) is adequate for studying non-covalent interactions dominated by dispersion effects like π -stacking.²⁷ In some complexes, we have also evaluated the noncovalent interactions using the RI-MP2/def2-TZVP level of theory in order to validate the DFT method used herein. We have used high spin configuration for the cobalt(III). The basis set superposition error for the calculation of interaction energies has been corrected using the counterpoise method.²⁸ The “atoms-in-molecules” (AIM) analysis of the electron density has been performed at the same level of theory using the AIMAll program.²⁹

We have also optimized the position of the hydrogen atoms of the crystal structures in order to compare the theoretically calculated (BP86-D3/def2-TZVP) positions to those obtained using isotopic thermal parameters (riding model). The positions of the hydrogen atoms are similar and consequently we have used the crystallographic ones. The geometries of the theoretically calculated complexes are included in the ESI.



Scheme 1: Syntheses of complexes **1** and **2**.

Catalytic oxidation of o-aminophenol

In order to examine the phenoxazinone synthase-like activity of the complexes, 1.02×10^{-5} M solutions of **1** and **2** in methanol were treated with a 10^{-3} M solution of o-aminophenol

(OAPH) under aerobic conditions at 25 °C. The reaction was followed spectrophotometrically by monitoring the increase in the absorbance as a function of time at ca. 433 nm, which is characteristic of the phenoxazinone chromophore. To determine the dependence of rate on the substrate concentration and various kinetic parameters, 1.02×10^{-5} M solutions of the complexes were mixed with at least 10 equivalents of substrate to maintain pseudo-first order conditions. Moreover, to check the rate dependency on catalyst concentration, a similar set of experiments was performed at a fixed concentration of substrate with varying amounts of catalyst. The rate of a reaction was derived from the initial rate method, and the average initial rate over three independent measurements was recorded.

Results and discussion

Syntheses

Schiff base ligand, HL (1-((2-(diethylamino)ethylimino)methyl)naphthalene-2-ol) was prepared by the 1:1 condensation of the 2-hydroxy-1-naphthaldehyde (HL') with N,N-diethylethylenediamine in methanol following the literature method.¹⁷ The methanol solution was then made to react with cobalt(II) acetate tetrahydrate and sodium azide in presence of two different coligands. In both cases octahedral cobalt(III) complexes **1** and **2** are formed when HL' and HL'' (acetylacetone) was used as coligands respectively.

Structure description of Complexes [Co(L)(N₃)(L')] (**1**) and [Co(L)(N₃)(L'')] (**2**)

Complex **1** crystallizes in tetragonal space group $P4_32_12$, whereas, complex **2** crystallizes in orthorhombic space group $P2_12_12_1$. Both the complex feature mononuclear octahedral cobalt(III) complex as shown in Figure 1. Selected bond lengths and bond angles of complexes

are given in Tables 2 and 3 respectively. In both the cases, central cobalt(III), Co(1), is coordinated meridionally by two nitrogen atoms, N(1) and N(2), and one oxygen atom, O(1), of the deprotonated Schiff base ligand (L^-) and two oxygen atoms, O(2) and O(3), of deprotonated coligand [$(L')^-$ for complex **1** and $(L'')^-$ for complex **2**]. Another nitrogen atom, N(3), of azide coordinates to complete the distorted octahedral geometry of cobalt(III). The saturated five membered rings [Co(1)–N(1)–C(23)–C(24)–N(2)] (for **1**) and [Co(1)–N(1)–C(12)–C(13)–N(2)] (for **2**) show envelope conformation on C(24) and C(13) with puckering parameters $q(2) = 0.453(3)\text{\AA}$, $\phi(2) = 113.1(3)^\circ$ and $q(2) = 0.445(3)\text{\AA}$, $\phi(2) = 115.5(3)^\circ$ respectively.³⁰

Supramolecular interactions and theoretical study

We have divided the theoretical study into two parts. In the first one we have analyzed the interesting C–H/ π and hydrophobic C–H \cdots H–C interactions observed in the solid state of complexes **1** and **2** that are crucial for understanding the final 3D architecture of the complexes. In the second part we have analyzed the counter intuitive chalcogen-chalcogen O \cdots O interactions observed in complex **1** involving two symmetrically related aldehyde groups of the ligand.

Both the aliphatic and aromatic parts of the tridentate ligand in complex **1** establish a variety of C–H/ π interactions in the solid state forming a supramolecular 1D chain (Figure 2A). Interestingly, the hydrogen atoms of the diethylamino group interact to one face of the π -system of the naphthalene moiety and concurrently the aromatic hydrogen atoms of the same ligand interact to the opposite face facilitating the formation of the 1D chain. We have studied this interaction using a dimeric model (Figure 2B) to keep the size of the system computationally approachable. We have computed the interaction energy of this dimer which is $\Delta E_1 = -17.5$

kcal/mol, which is large because of the enhanced acidity of the interacting hydrogen atoms due to the coordination of the ligand to the cobalt(III) metal center that strengthens the C–H/ π interactions. As a matter of fact, if the calculations are performed without the cobalt(III) transition metal (protonating the ligand to keep the model neutral), the interaction energy is reduced to -7.5 kcal/mol for the aliphatic and to -5.2 kcal/mol for the aromatic C–H/ π interaction. To corroborate this explanation, we have computed the atomic charges of the interacting hydrogen atoms, which are 0.17 and 0.19 e for the aliphatic and aromatic hydrogen atoms, respectively, when the ligand is coordinated to cobalt(III). The charges are reduced to 0.15 e (for both hydrogen atoms) when the ligand is not coordinated, thus supporting the acidity enhancement of the interacting hydrogen atoms of the ligand upon complexation.

In addition to the C–H/ π bonding network, non-covalent C–H \cdots H–C interactions are also observed in the solid state of complex **1** (see Figure 3) in the formation of a self-assembled dimer where the azide coligand also participates establishing hydrogen bonding interactions. Recently a combined computational and CSD study has demonstrated the importance of C–H \cdots H–C interactions weak interactions in the solid state.³¹ In fact the binding energy of the dimer of dodecahedrane,³¹ that is stabilized only by C–H \cdots H–C interactions, is approximately 3 kcal/mol. To further analyze the importance on this interaction, we have computed the binding energies in a series of theoretical dimers based on the X-ray structure (see Figure 3). In Figure 3B the dimer retrieved from the X-ray geometry is shown where, in addition to the C–H \cdots H–C interactions, a hydrogen bonding network with the participation of the azide and aldehyde moieties is present. The interaction energy of this dimer is very large and negative ($\Delta E_2 = -20.9$ kcal/mol) due to the hydrogen bonding interactions. We have also computed a theoretical model where the azide coligands have been replaced by hydrides (Figure 3C) and consequently the hydrogen bonding

interactions involving azide are not present. As a result the interaction energy is significantly reduced to $\Delta E_3 = -12.7$ kcal/mol that corresponds to the hydrogen bonding interactions established between the symmetrically related aldehyde groups [coordinated to cobalt(III)] and the C–H...H–C interactions. Moreover, we have computed another theoretical model where the azide coligands and the ethyl substituents of the amino group have been replaced by hydrides and hydrogen atoms, respectively (Figure 3D) and consequently only the hydrogen bonding interaction involving coordinated aldehyde groups are evaluated. As a result the interaction energy is further reduced to $\Delta E_4 = -6.9$ kcal/mol that corresponds to both complementary CO...HC hydrogen bonding interactions. The contribution of the C–H...H–C interaction can be evaluated as $\Delta E_{\text{C-H...H-C}} = \Delta E_4 - \Delta E_3 = -5.8$ kcal/mol. The large binding energy for this interaction can be rationalized by means of the large number of individual and additive C–H...H–C contacts. Similar results have been observed in long open chain alkanes, where the number of side-on contacts between neighbouring molecules increases resulting in large dimer dissociation energies, as high as 4.5 kcal/mol for n-hexane.^{31b}

It can be observed in Figure 3 that the O...O distance between the oxygen atoms of the coordinated aldehyde groups is shorter than the sum of van der Waals radii ($\sum R_{\text{vdW}} = 3.04$ Å). We have investigated the physical nature of this counterintuitive “like-like” interaction between the oxygen atoms (red dashed line in Figure 3). We have first computed the non-covalent interaction (NCI) plot of the dimer of **1** using the crystallographic coordinates to analyze the intermolecular non-covalent interactions. The NCI plot is a visualization index based on the electron density and its derivatives, and enables identification and visualization of non-covalent interactions efficiently. The isosurfaces correspond to both favorable and unfavorable interactions, as differentiated by the sign of the second density Hessian eigenvalue and defined

by the isosurface color. NCI analysis allows an assessment of host-guest complementarity and the extent to which weak interactions stabilize a complex. The information provided by NCI plots is essentially qualitative, i.e. which molecular regions interact. The color scheme is a red-yellow-green-blue scale with red for ρ^+_{cut} (repulsive) and blue for ρ^-_{cut} (attractive). Yellow and green surfaces correspond to weak repulsive and weak attractive interactions, respectively.³² In Figure 4A we show the representation of the NCI plot computed for the dimer. It can be observed a region between the ethyl groups that confirm the existence of favorable C–H...H–C interactions. In addition, there is long isosurface that corresponds to the hydrogen bonding network in the region of the azide ligand. Finally there is also a green surface in the region where the aldehyde groups interact. In order to further analyze the aldehyde-aldehyde interaction we have optimized a model dimer using formaldehyde and the interaction energy is $\Delta E_5 = -1.6$ kcal/mol that is modest (Figure 4B). Since this value is small, we have also computed the interaction energy at a higher level of theory, i.e. CCSD(T)/def2-TZVP. As a result, the interaction energy is similar (-1.3 kcal/mol), giving reliability to the DFT-D3 method. Moreover, we have also used the symmetry adapted perturbation theory (SAPT)^{33a} to provide quantitative information on the magnitude of the electrostatic, induction and dispersion interactions. For the formaldehyde dimer complex the DFT-SAPT method gives a total interaction energy of $E_t(\text{SAPT}) = -1.0$ kcal/mol, that is in reasonable agreement with the CCSD(T) interaction energy. The partitioning of the interaction energy into the individual contributions is as follows: electrostatic term is $E_{\text{ele}} = -2.4$ kcal/mol, exchange term is $E_{\text{exc}} = +3.1$ kcal/mol, induction term is $E_{\text{ind}} = -0.2$ and dispersion term is $E_{\text{disp}} = -1.5$ kcal/mol. Therefore the aldehyde-aldehyde interaction is dominated by the electrostatic and dispersion terms. Strikingly the AIM analysis shows that the interaction is characterized by a bond critical point (red sphere) and a bond path

that connects both oxygen atoms confirming the existence of chalcogen-chalcogen interaction. The distribution of critical points does not show a bond critical point connecting the hydrogen to the oxygen atoms. It should be mentioned that the optimized O...O distance (2.98 Å) is very similar to the distance observed in the X-ray structure (2.94 Å). We have also analyzed how the interaction energy is affected by the O...O distance (Table 4). The interaction energy is reduced in more than 50% upon increasing 0.5 Å the O...O distance. At this point, in order to investigate the O...O interaction from an orbital point of view we have performed Natural Bond Orbital (NBO)^{33b} calculations in the formaldehyde dimer focusing our attention on the second order perturbation analysis that is very useful to study donor acceptor interactions. Interestingly, we have found that the lone pair (lp orbital) of one oxygen atom interacts with the C–O and C–H antibonding orbitals of the opposite formaldehyde anion and *vice-versa* with a concomitant second order stabilization energy of $E^{(2)} = 0.18$ kcal/mol for each interaction. In addition the energetic differences between the lp and σ^* orbitals are only 0.50 and 0.75 a.u. for the C–H and C–O bonds, respectively. Therefore the orbital stabilization energy that can be attributed to the O...O is approximately 0.34 kcal/mol in the dimer. We have also computed the AIM analysis of the model dimer of complex **1** shown in Figure 3C in order to investigate if the distribution of critical points is similar to the one found in the formaldehyde dimer. The distribution is shown in Figure 5A. It can be observed that the distribution in this model of complex **1** also exhibits two bond critical points that characterize the hydrogen bonds in addition to the bond CP and bond path that characterize the O...O interaction. This results agrees with the larger binding energy obtained for the dimer of complex **1** compared to the formaldehyde dimer. The properties of the charge density at the bond CPs are summarized in Table 5. The values of the Laplacian are positive as is common in closed shell interactions. The Kinetic energy and the total energy

density are higher at the bond CP that connects the oxygen atoms than that at the bond CP that characterizes the hydrogen bonds. Finally, we also represent in Figure 5B the distribution of critical points that characterizes the C–H...H–C interaction described above (see Figure 3A). This interaction is characterized by the presence of three bond CPs and bond paths that interconnect three hydrogen atoms of the ethyl groups.

For complex **2** we have focused our attention to the C–H/ π interactions and the influence of the metal center of the strength of the interaction. The dimers retrieved from the X-ray structure are shown in Figure 6. In one dimer the hydrogen atoms that participate in the interaction belong to the aliphatic part of the tridentate Schiff base ligand (Figure 6A) and in the other dimer the hydrogen atoms belong to the acetylacetonate (4-oxopent-2-en-2-olate) coligand (Figure 6B). The interaction energies of the dimers are $\Delta E_6 = -11.1$ kcal/mol for the Schiff base interaction and $\Delta E_7 = -8.2$ kcal/mol for the acetylacetonate coligand. We have used two theoretical models to evaluate the influence of the coordination to the transition metal upon the interaction energies. In both models we have eliminated the metal center and protonated the oxygen atom of the ligand that is coordinated to the cobalt(III) ion in the real system (Figure 6C and D). As a result both interaction energies weaken to $\Delta E_8 = -6.0$ kcal/mol and $\Delta E_9 = -6.1$ kcal/mol, confirming that the coordination of the ligand to the metal center increases the acidity of the interacting hydrogen atoms and enhances the C–H/ π interactions. For the latter models we have also computed the interaction energy at a higher level of theory (RI-MP2) in order to validate the DFT method used in this study. The interaction energies are in reasonable agreement, giving reliability to the methodology used herein (Figure 6).

We have also confirmed the existence of the aforementioned C–H/ π interactions using the AIM analysis of critical points and bond paths (Figure 7). In the dimer where the interacting

hydrogen atoms belong to the aliphatic part of the tridentate Schiff base ligand (Figure 7A) the distribution of critical points show four bond CPs that connect several hydrogen atoms with the carbon atoms of the aromatic rings. The interaction is further characterized by the presence of several ring CPs that are generated as a consequence of the formation of several supramolecular rings. In the other dimer the hydrogen atoms belong to the acetylacetonate coligand (Figure 7B) and the interaction is characterized by the presence of three bond CPs that connect three hydrogen atoms with three carbon atoms of the aromatic part of the ligand. The interaction is further characterized by the presence of two ring CPs. The properties of the density at two representative bond CPs are summarized in Table 5.

Phenoxazinone synthase like activity

The phenoxazinone synthase mimicking activity of the complex **2** was studied by monitoring the oxidation of o-aminophenol (OAPH) spectrophotometrically in dioxygen saturated methanol solution at room temperature. Before going into detailed kinetic investigation, it is necessary to get an estimation of the ability of the complexes to oxidize o-aminophenol, and for this purpose 1.0×10^{-5} M solutions of the complexes were mixed with a 10^{-3} M solution of OAPH, and the spectra were recorded for up to 2 h in dioxygen saturated methanol at room temperature. The time dependent spectral profiles for a period of 2 h after the addition of OAPH are shown in Figure 8 for **2**. The spectral scans reveal the progressive increase of peak intensity at ca. 433 nm, characteristic of the phenoxazinone chromophore, suggesting the catalytic conversion of OAPH to 2-aminophenoxazine-3-one in aerobic conditions. A blank experiment without catalyst under identical conditions does not show significant growth of the

band at 433 nm. These spectral behaviors conclude that complex **2** show phenoxazinone synthase-like activity under aerobic conditions.

Kinetic studies were performed to understand the extent of the catalytic efficiency. For this purpose, 1.0×10^{-5} M solutions of the complex was treated with substrate, maintaining pseudo first order conditions. For a particular complex substrate mixture, time scans at the maximum band of 2-aminophenoxazine-3-one were carried out for a period of 30 min, and the initial rate was determined by linear regression from the slope of the absorbance versus time, and each experiment was performed thrice and average values were noted. As shown in Figure 9, the initial rates of the reaction versus concentration of the substrate plots show rate saturation kinetics. This observation indicates that an intermediate complex substrate adduct formed at a preequilibrium stage and that the irreversible substrate oxidation is the rate determining step of the catalytic cycle. This type of saturation rate dependency on the concentration of the substrate can be treated with the Michaelis–Menten model, which upon linearization gives a double reciprocal Lineweaver–Burk plot to analyze values of the parameters V_{\max} , K_M , and K_{cat} . The observed and simulated initial rates versus substrate concentration plot and the Lineweaver–Burk plot for **2** are shown in Figure 9 and 10, respectively. Analysis of the experimental data yielded Michaelis binding constant (K_M) value of 4.39×10^{-3} and V_{\max} value of $8.09 \times 10^{-5} \text{ M}^{-1}$. The turnover number (K_{cat}) value is obtained by dividing the V_{\max} by the concentration of the complex used, and is found to be 8.32 s^{-1} .

IR and NMR spectra

In the IR spectra of **1** and **2** distinct bands due to azomethine (C=N) groups appear at 1583 and 1577 cm^{-1} respectively whereas, bands for carbonyl (C=O) groups are noticed at 1618,

and 1621 cm^{-1} respectively.^{34,35} Appearance of strong band at 2023 cm^{-1} in the IR spectra of both complexes indicates the presence of azide.³⁶

^1H NMR spectra data for complexes **1** and **2** have been summarized in experimental section and the spectra have been depicted in Figure S1 and 11 respectively. Imine protons ($-\text{CH}=\text{N}$) of **1** and **2** appear as a singlet at 8.83 ppm and 8.72 ppm respectively whereas, aldehyde protons ($-\text{CH}=\text{O}$) of **1** appears at 9.77 ppm. A sharp singlet at 5.62 ppm and two sharp singlet at 2.27 ppm and 1.63 ppm appears in the spectrum of **2** suggesting the presence of acetylacetonate moiety (Figure 11).

Electronic spectra and photophysical study

In electronic spectra of both complexes, two absorption bands of similar fashion are observed at 404 nm, 421 nm (for **1**, see Figure S2) and 408 nm, 424 nm (for **2**, see Figure S3) in the visible region which are assigned as LMCT.³⁴ In UV region few other absorption bands are observed at 220 nm, 269 nm, 319 nm for **1** and 224, 266 for **2**. These bands are attributed to $\pi\text{-}\pi^*$ transition of azomethine and naphthalene chromophores. No d-d bands are observed at higher wavelength in the electronic spectra of both complexes. The bands are not observed due to the low concentration ($10^{-4}\text{ mol L}^{-1}$) of the complexes solution. These bands should be low in intensity in the region of 500-600 nm.

Complex **1** shows emission at 344 nm in the UV region, whereas complex **2** exhibits emission in the visible region at 431 nm upon irradiation with UV-light (300 nm) in acetonitrile at room temperature (Figure 12). The excited state mean lifetimes of complexes **1** and **2** are 3.17 ns and 6.7 ns respectively. This emission band can be attributed to intra ligand fluorescent $^1(\pi\rightarrow\pi^*)$ emission of the coordinated ligand.³⁷

Relative fluorescence quantum yields for two complexes were measured in acetonitrile using quinine sulfate (in 0.5 (M) H₂SO₄, $\Phi = 0.54$) as the quantum yield standard.³⁸ The fluorescence quantum yields of complexes **1** and **2** are 0.0046, 0.0041 respectively. If Φ_x and Φ_s are the quantum yields of a given fluorophore species 'x' and the standard 's', respectively, then

$$\Phi_x = \Phi_s(F_x/F_s)(A_x/A_s)$$

where F_x , F_s are the wavelength integrated emission intensities of the two samples, A_s , A_x are the optical densities at their corresponding wavelengths of excitation.³⁹

Conclusion

Herein, we report the synthesis, X-ray characterization and photoluminescence properties of two new coordination cobalt(III) Schiff base complexes. Hydrogen bonding, C–H/ π and O \cdots O interactions play an important role in the packing of the complexes in the solid state. The metal coordination of the ligands enhances the C–H/ π interaction as has been demonstrated by means of DFT calculations. A special attention has been paid to the short O \cdots O interactions between the aldehyde groups that has been analyzed using a variety of computational tools. It has a favorable orbital contribution that is rationalized by means of donor-acceptor orbital interactions (lp \rightarrow σ^* electron donation).

Acknowledgments

S.C. acknowledges DST, India under FAST Track Scheme (Order No. SR/FT/CS-118/2010, dated 15/02/2012). K.R. gratefully acknowledges the financial support from the Academy of Finland (Project No's. 122350, 140718, 256259, 265328 and 263256). A.B. and

A.F. thank MINECO of Spain (project CONSOLIDER INGENIO 2010 CSD2010-00065, FEDER funds) and the CTI (UIB) for free allocation of computer time.

References

- 1 (a) Y.-Y. Zhu, C. Cui, Y.-Q. Zhang, J.-H. Jia, X. Guo, C. Gao, K. Qian, S.-D. Jiang, B.-W. Wang, Z.-M. Wang and S. Gao, *Chem. Sci.*, 2013, **4**, 1802–1806; (b) S. Biswas, A. Dutta, M. Debnath, M. Dolai, K. K. Das and M. Ali, *Dalton Trans.*, 2013, **42**, 13210–13219; (c) X. Zhang, C. B. Sangani, L.-X. Jia, P.-X. Gong, F. Wang, J.-F. Wang and H.-L. Zhu, *RSC Adv.*, 2014, **4**, 54217–54225; (d) X. Dong, T. Guo, Y. Li, Y. Cui and Q. Wang, *J. Inorg. Biochem.*, 2013, **127**, 82–89; (e) Y. J. Na, G. J. Park, H. Y. Jo, S. A. Lee and C. Kim, *New J. Chem.*, 2014, **38**, 5769–5776; (f) X.-J. Jiang, M. Li, H.-L. Lu, L.-H. Xu, H. Xu, S.-Q. Zang, M.-S. Tang, H.-W. Hou and T. C. W. Mak, *Inorg. Chem.*, 2014, **53**, 12665–12667; (g) T.-T. Wang, M. Ren, S.-S. Bao and L.-M. Zheng, *Eur. J. Inorg. Chem.*, 2014, 1042–1050.
- 2 (a) M. Á. Vázquez-Fernández, M. R. Bermejo, M. I. Fernández-García, G. González-Riopedre, M. J. Rodríguez-Doutón and M. Maneiro, *J. Inorg. Biochem.*, 2011, **105**, 1538–1547; (b) P. Seth, L. K. Das, M. G. B. Drew and A. Ghosh, *Eur. J. Inorg. Chem.*, 2012, 2232–2242; (c) A. Panja, *Dalton Trans.*, 2014, **43**, 7760–7770; (d) M. Shyamal, T. K. Mandal, A. Panja and A. Saha, *RSC Adv.*, 2014, **4**, 53520–53530.
- 3 (a) M. D. Peterson, R. J. Holbrook, T. J. Meade and E. A. Weiss, *J. Am. Chem. Soc.*, 2013, **135**, 13162–13167; (b) S. Thakurta, J. Chakraborty, G. Rosair, R. J. Butcher and S. Mitra, *Inorg. Chim. Acta*, 2009, **362**, 2828–2836.
- 4 (a) A. C. Rizzi, C. D. Brondino, R. Calvo, R. Baggio, M. T. Garland and R. E. Rapp, *Inorg. Chem.*, 2003, **42**, 4409–4416; (b) J. S. Miller, M. Drillon (Eds.), *Magnetism: Molecules to Materials IV*, Wiley–VCH, Weinheim, Germany, 2003; (c) B. S. Snyder, G. S. Patterson, A. J. Abrahamson and R. H. Holm, *J. Am. Chem. Soc.*, 1989, **111**, 5214–5223; (d) C. Fraser and B. Bosnich, *Inorg. Chem.*, 1994, **33**, 338–346; (e) V. G. Makhankova, O. Y. Vassilyeva, V. N.

Kokozay, B. W. Skelton, L. Sorace and D. Gatteschi, *J. Chem. Soc., Dalton Trans.*, 2002, 4253-4259; (f) L. Sacconi, M. Ciampolini and G. P. Speroni, *Inorg. Chem.*, 1965, **4**, 1116-1119; (g) R. Dreos, G. Nardin, L. Randaccio, P. Siega, G. Tauzher and V. Vrdoljak, *Inorg. Chim. Acta*, 2003, **349**, 239-248.

5 (a) S. Yamada, *Coord. Chem. Rev.*, 1999, **191**, 537-555; (b) N. J. Henson, P. J. Hay and A. Redondo, *Inorg. Chem.*, 1999, **38**, 1618-1626.

6 (a) P. K. Mascharak, *Coord. Chem. Rev.*, 2002, **225**, 201-214; (b) D. P. Kessissoglou, *Coord. Chem. Rev.*, 1999, **185**, 837-858; (c) H. Chen, D. Han, H. Yan, W. Tang, Y. Yang and H. Wang, *Polyhedron* 1993, **12**, 1097-1099; (d) S. Thakurta, R. J. Butcher, G. Pilet and S. Mitra, *J. Mol. Struct.*, 2009, **929**, 112-119 (and references therein).

7 (a) A. D. Khalaji, M. Nikookar, K. Fejfarova and M. Dusek, *J. Mol. Struct.*, 2014, **1071**, 6-10; (b) M. Y. Nassar, T. Y. Mohamed and I. S. Ahmed, *J. Mol. Struct.*, 2013, **1050**, 81-87; (c) M. Salavati-Niasari, A. Khansari and F. Davar, *Inorg. Chim. Acta*, 2009, **362**, 4937-4942.

8 (a) R. S. Forgan, R. J. Marshall, M. Struckmann, A. B. Bleine, D.-L. Long, M. C. Berninib and D. Fairen-Jimenez, *CrystEngComm*, 2015, **17**, 299-306; (b) B. Nepal and S. Scheiner, *Chem. Eur. J.*, 2015, **21**, 1474-1481; (c) C. Prez, D. P. Zaleski, N. A. Seifert, B. Temelso, G. C. Shields, Z. Kisiel and B. H. Pate, *Angew. Chem. Int. Ed.*, 2014, **53**, 14368 -14372.

9 (a) D. L. Reger, A. Leitner, P. J. Pellechia, and M. D. Smith, *Inorg. Chem.*, 2014, **53**, 9932-9945; (b) L. Liu, J. Hao, Y. Shi, J. Qiu and C. Hao, *RSC Adv.*, 2015, **5**, 3045-3053; (c) K. K. Bania, A. K. Guha, P. K. Bhattacharyya and S. Sinha, *Dalton Trans.*, 2014, **43**, 1769-1784; (d) S. Yamada, N. Sako, M. Okuda and A. Hozumi, *CrystEngComm*, 2013, **15**, 199-205; (e) M. K. Singh and G. Rajaraman, *Chem. Eur. J.*, 2015, **21**, 980-983; (f) X. Xu, B. Pooi, H. Hirao and S. H. Hong, *Angew. Chem. Int. Ed.*, 2014, **53**, 1283 -1287.

10 (a) S. Guha and S. Saha, *J. Am. Chem. Soc.*, 2010, **132**, 17674–17677; (b) J.-J. Liu, Y.-J. Hong, Y.-F. Guan, M.-J. Lin, C.-C. Huang and W.-X. Dai, *Dalton Trans.*, 2015, **44**, 653–658; (c) D.-X. Wang and M.-X. Wang, *J. Am. Chem. Soc.*, 2013, **135**, 892–897; (d) T. Korenaga, T. Shoji, K. Onoue and T. Sakai, *Chem. Commun.*, 2009, 4678–4680; (e) A. Frontera, P. Gamez, M. Mascal, T. J. Mooibroek and J. Reedijk, *Angew. Chem. Int. Ed.* 2011, **50**, 9564–9583; (f) A. Bauzá and A. Frontera, *Angew. Chem. Int. Ed.*, 2015, **54**, 7340–7343; (g) A. Bauzá, T. J. Mooibroek and A. Frontera, *Angew. Chem. Int. Ed.*, 2013, **52**, 12317–12321; (h) A. Bauzá, T. J. Mooibroek and A. Frontera, *Chem Eur. J.*, 2014, **20**, 10245–10248; (i) A. Bauzá, T. J. Mooibroek and A. Frontera, *ChemPhysChem.*, 2015, **16**, 10.1002/cphc.201500314.

11 (a) M. Bai, S. P. Thomas, R. Kottokkaran, S. K. Nayak, P. C. Ramamurthy and T. N. G. Row, *Cryst. Growth Des.*, 2014, **14**, 459–466 (and references therein); (b) F. V. González, A. Jain, S. Rodríguez, J. A. Sáez, C. Vicent and G. Peris, *J. Org. Chem.*, 2010, **75**, 5888–5894; (c) C. Ji, J. D. Goddard and A. Houmam, *J. Am. Chem. Soc.*, 2004, **126**, 8076–8077.

12 (a) Y. Nagao, T. Hirata, S. Goto, S. Sano, A. Kakehi, K. Iizuka and M. Shiro, *J. Am. Chem. Soc.*, 1998, **120**, 3104–3110; (b) A. S. Batsanov, *Acta Cryst.*, 2006, **C62**, o501–o504.

13 (a) Y. Bian, J. Chen, S. Xu, Y. Zhou, L. Zhu, Y. Xiang and D. Xia, *New J. Chem.*, 2015, **39**, 5750–5758. (b) D. J. Wolstenholme, J. L. Dobson and G. S. McGrady, *Dalton Trans.*, 2015, **44**, 9718–9731.

14 (a) S. Jana, K. Harms, A. Bauza, A. Frontera and S. Chattopadhyay, *Cryst. Growth Des.*, 2015, **15**, 257–267. (b) A. Bhattacharyya, P. K. Bhaumik, A. Bauza, P. P. Jana, A. Frontera, M. G. B. Drewd and S. Chattopadhyay, *RSC Adv.*, 2014, **4**, 58643–58651.

15 R. F. W. Bader, *Chem. Rev.*, 1991, **91**, 893–928.

- 16 F. Weinhold and C. R. Landis, *Valency and Bonding - A Natural Bond Orbital Donor-Acceptor Perspective* Cambridge University Press, 2005.
- 17 M. Das and S. Chattopadhyay, *J. Mol. Struct.*, 2013, **1051**, 250–258.
- 18 R. W. Hooft, Collect, Nonius BV, Delft, The Netherlands, 1998.
- 19 Z. Otwinowski and W. Minor, *Methods in Enzymology*, 1997, 276, Macromolecular Crystallography, Part A, 307.
- 20 G. M. Sheldrick, SADABS, Bruker Analytical X-ray system Inc, Madison, Wisconsin, 2008.
- 21 CrysAlisPro, Agilent Technologies. Version 1.171.36.21, 2012.
- 22 R. C. Clark and J. S. Reid, *Acta Cryst.*, 1995, **A51**, 887-897.
- 23 L. Palatinus and G. Chapuis, *J. Appl. Crystallogr.*, 2007, **40**, 786-790.
- 24 L. J. Farrugia, *J. Appl. Crystallogr.*, 1999, **32**, 837-838.
- 25 G. M. Sheldrick, *Acta Cryst.*, 2008, **A64**, 112-122.
- 26 R. Ahlrichs, M. Bär, M. Hacer, H. Horn and C. Kömel, *Chem. Phys. Lett.*, 1989, **162**, 165–169.
- 27 S. Grimme, J. Antony, S. Ehrlich and H. Krieg, *J. Chem. Phys.*, 2010, **132**, 154104-19
- 28 S. B. Boys and F. Bernardi, *Mol. Phys.*, 1970, **19**, 553–566.
- 29 AIMAll (Version 13.05.06), Todd A. Keith, TK Gristmill Software, Overland Park KS, USA, 2013.
- 30 D. Cremer and J. A. Pople, *J. Am. Chem. Soc.*, 1975, **97**, 1354-1358.
- 31 (a) J. Echeverría, G. Aullón, D. Danovich, S. Shaik and S. Alvarez, *Nature Chem.*, 2011, **3**, 323–330. (b) S. Tsuzuki, K. Honda, U. Tadafumi and M. Mikami, *J. Phys. Chem. A*, 2004, **108**, 10311–10316. (c) M. Mirzaei, M. Nikpour, A. Bauzá and A. Frontera, *ChemPhysChem*, 2015, **16**, 2260–2266.

- 32 J. Contreras-García, E. R. Johnson, S. Keinan, R. Chaudret, J. P. Piquemal, D. N. Beratan and W. Yang, *J. Chem. Theory and Comput.*, 2011, **3**, 625-632.
- 33 (a) B. Jeziorski, R. Moszynski and K. Szalewicz, *Chem. Rev.*, 1994, **94**, 1887. (b) F. Weinhold, *J. Comput. Chem.*, 2012, **33**, 2363–2379.
- 34 R. Taherlo and M. Salehi, *Inorg. Chim. Acta*, 2014, **418**, 180–186.
- 35 K. Nakamoto, P. J. McCarthy, A. Ruby and A. E. Martell, *J. Am. Chem. Soc.*, 1961, **83**, 1066-1069.
- 36 S. Jana, P. K. Bhaumik, K. Harms and S. Chattopadhyay, *Polyhedron*, 2014, **78**, 94–103.
- 37 S. H. Rahaman, H. Chowdhury, H. L. Milton, A. M. Z. Slawin, J. Derek Woollins and B. K. Ghosh, *Inorg. Chem. Commun.*, 2005, **8**, 1031–1035.
- 38 R. A. Velapoldi, K. D. Mielenz, *Standard Reference Materials: A Fluorescence Standard Reference Material: Quinine Sulfate Dihydrate*, National Bureau of Standards Special Publication 260-64, National Bureau of Standards, Washington, DC, 1980
- 39 J. R. Lakowicz, *Principles of Fluorescence Spectroscopy*, third ed., SpringerVerlag, New York, 2006.

Table 1: Crystal data and refinement details in complexes **1** and **2**

Complexes	1	2
Formula	C ₂₈ H ₂₈ CoN ₅ O ₃	C ₂₂ H ₂₈ CoN ₅ O ₃
Formula Weight	541.48	469.42
Crystal Size (mm)	0.12 x 0.18 x 0.24	0.14 x 0.21 x 0.32
Temperature (K)	123	170
Crystal system	Tetragonal	Orthorhombic
Space group	<i>P</i> 4 ₃ 2 ₁ 2	<i>P</i> 2 ₁ 2 ₁ 2 ₁
a(Å)	10.2252(2)	9.55072(15)
b(Å)	10.2252(2)	12.7917(2)
c(Å)	50.0545(10)	18.0663(3)
Z	8	4
<i>d</i> _{calc} (g cm ⁻³)	1.375	1.413
μ (mm ⁻¹)	5.459	0.811
<i>F</i> (000)	2256	984
Total Reflections	9712	28107
Unique Reflections	4839	5055
Observed data [<i>I</i> > 2σ (<i>I</i>)]	4405	4429
R(int)	0.051	0.056
R1, wR2 (all data)	0.0442, 0.0940	0.0472, 0.0845
R1, wR2 [<i>I</i> > 2 σ (<i>I</i>)]	0.0403, 0.0927	0.0364, 0.0782
Largest diff. in peak and hole (eÅ ⁻³)	0.33, -0.21	0.36, -0.25

Table 2: Selected bond lengths around cobalt(III) (Å) in complexes **1** and **2**.

Complex	1	2
Co(1)–O(1)	1.894(2)	1.874(2)
Co(1)–O(2)	1.909(2)	1.922(2)
Co(1)–O(3)	1.909(2)	1.915(2)
Co(1)–N(1)	1.883(2)	1.887(2)
Co(1)–N(2)	2.068(2)	2.066(2)
Co(1)–N(3)	1.932(2)	1.949(2)

Table 3: Selected bond angles around cobalt(III) (°) in complexes **1** and **2**.

Complex	1	2
O(1)–Co(1)–O(2)	89.75(9)	87.60(7)
O(1)–Co(1)–O(3)	87.33(8)	86.03(7)
O(1)–Co(1)–N(1)	93.56(8)	93.49(8)
O(1)–Co(1)–N(2)	176.66(8)	179.02(8)
O(1)–Co(1)–N(3)	88.74(1)	90.68(8)
O(2)–Co(1)–O(3)	92.32(8)	93.87(7)
O(2)–Co(1)–N(1)	87.52(8)	88.61(8)
O(2)–Co(1)–N(2)	93.58(8)	93.19(8)
O(2)–Co(1)–N(3)	178.11(9)	178.28(8)
O(3)–Co(1)–N(1)	179.10(9)	177.46(8)
O(3)–Co(1)–N(2)	92.85(9)	94.51(8)
O(3)–Co(1)–N(3)	86.49(9)	85.85(8)
N(1)–Co(1)–N(2)	86.28(9)	85.94(8)
N(1)–Co(1)–N(3)	93.69(9)	91.66(9)
N(2)–Co(1)–N(3)	87.95(1)	88.53(8)

Table 4: Interaction energy (BSSE corrected) of the formaldehyde dimer at different distances

O...O distance (Å)	ΔE (kcal/mol)
2.98	-1.6
3.06	-1.5
3.21	-1.0
3.46	-0.7

Table 5: Properties (a.u.) at the bond critical point for some model dimers of complexes **1** and **2**.

See Figures 5 and 7 and for the labelling of critical points.

Complex	ρ	$\nabla^2\rho$	H(r)	G(r)	V(r)	ϵ
CP1	0.0092	0.0387	0.0019	0.0078	-0.0059	0.4139
CP2	0.0090	0.0420	0.0021	0.0084	-0.0064	0.7379
CP3	0.0050	0.0206	0.0013	0.0039	-0.0026	0.1496
CP4	0.0051	0.0206	0.0013	0.0039	-0.0027	0.1395
CP5	0.0042	0.0155	0.0008	0.0031	-0.0023	0.0594
CP6	0.0057	0.0154	0.0006	0.0032	-0.0026	0.3015
CP7	0.0043	0.0128	0.0007	0.0025	-0.0019	0.6784

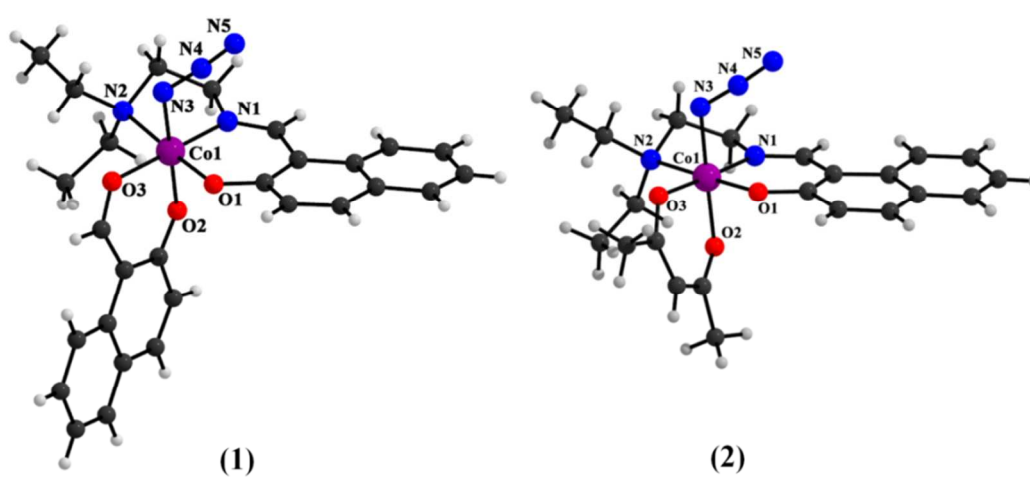


Figure 1: Perspective views of complexes 1 and 2 with selective atom numbering scheme.

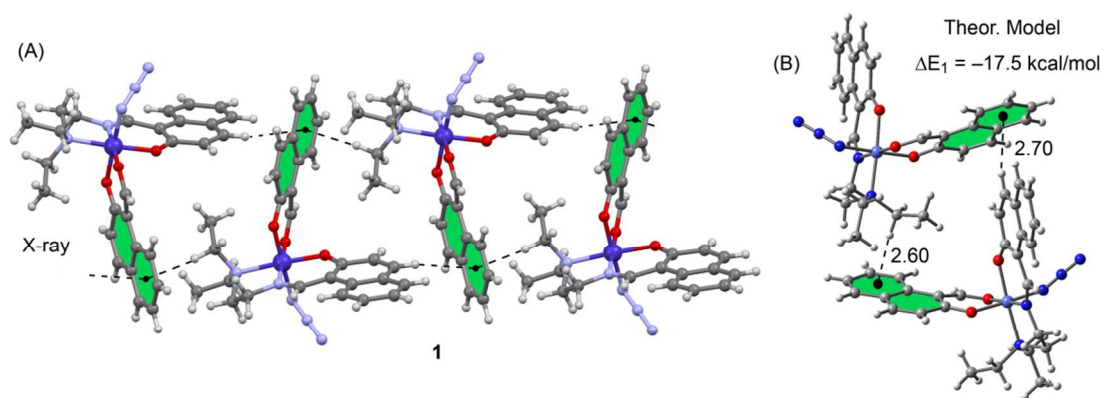


Figure 2: (A) X-ray fragment of complex **1**. (B) Theoretical model used to estimate the C–H/ π interactions. Distances in Å

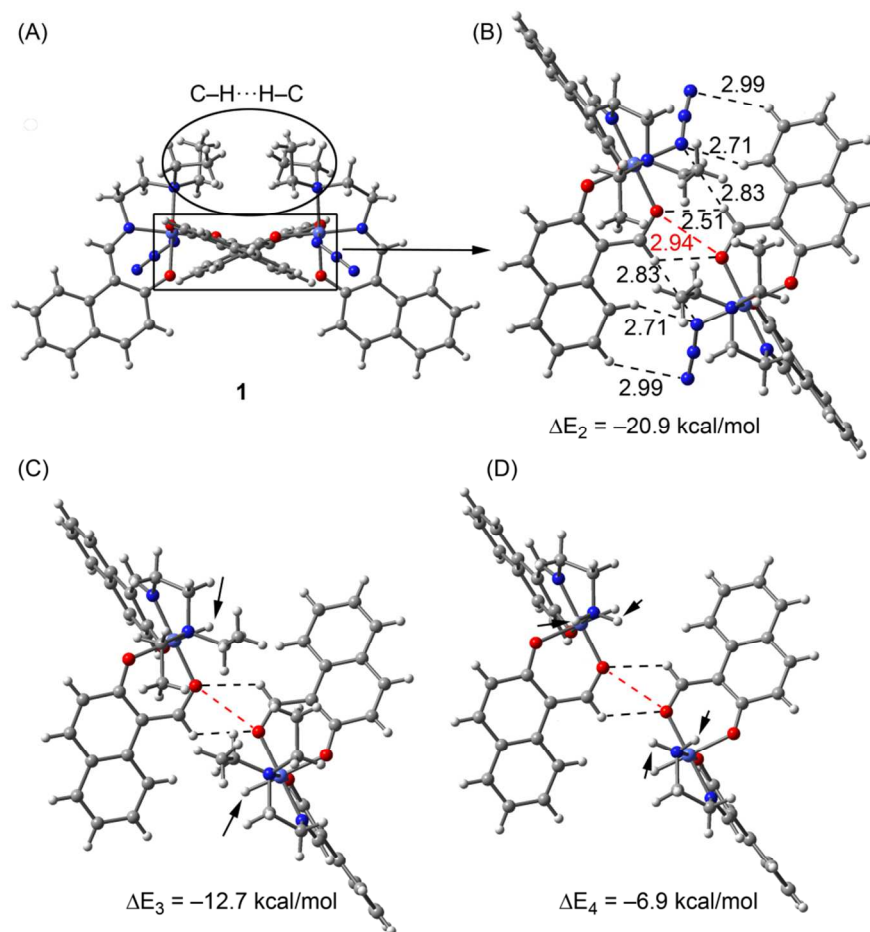


Figure 3: Theoretical model used to estimate the $C-H \cdots H-C$ and hydrogen bonding interactions. Distances in Å

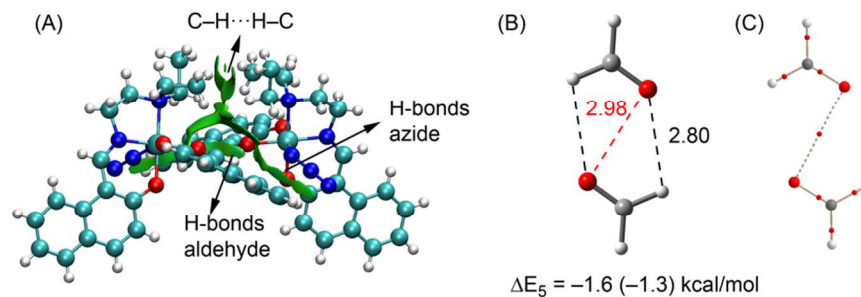


Figure 4: (A) NCI plot of the dimer of complex **1**. (B) Optimized dimer of formaldehyde at the BP86-D3/def2-TZVP level of theory, value in parenthesis corresponds to the energy at the CCDC(T)/def2-TZVP. Distances are in Å. (C) Distribution of critical points and bond paths in the formaldehyde dimer.

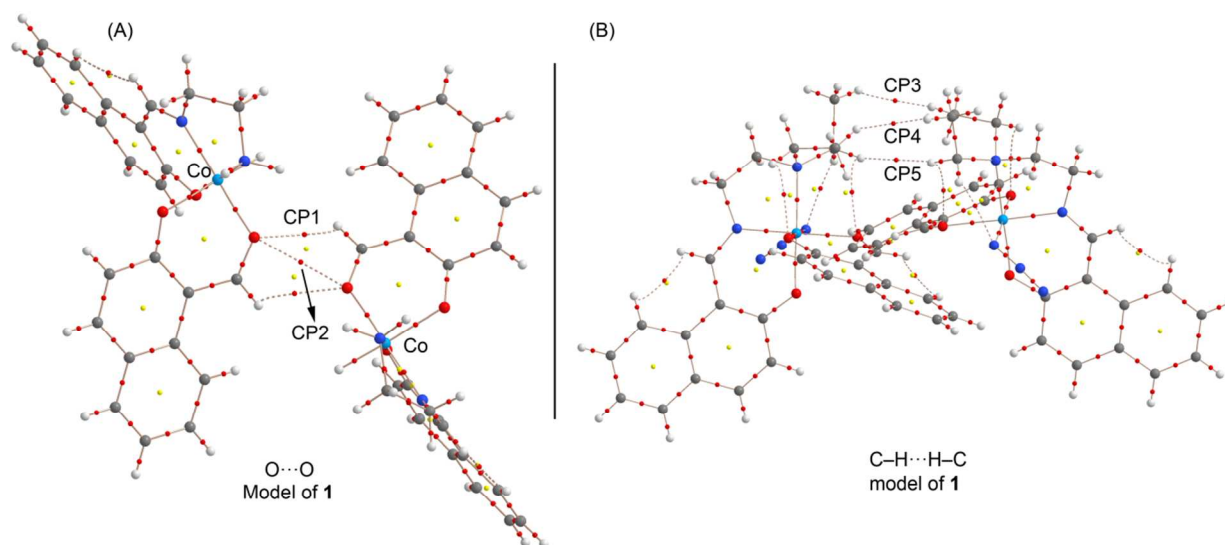


Figure 5. Distribution of bond and ring critical points (red and yellow spheres, respectively) and bond paths in two dimers of complex **1**. In Figure 5B only the intermolecular bond CPs that characterize the C–H...H–C interaction are represented for the sake of clarity.

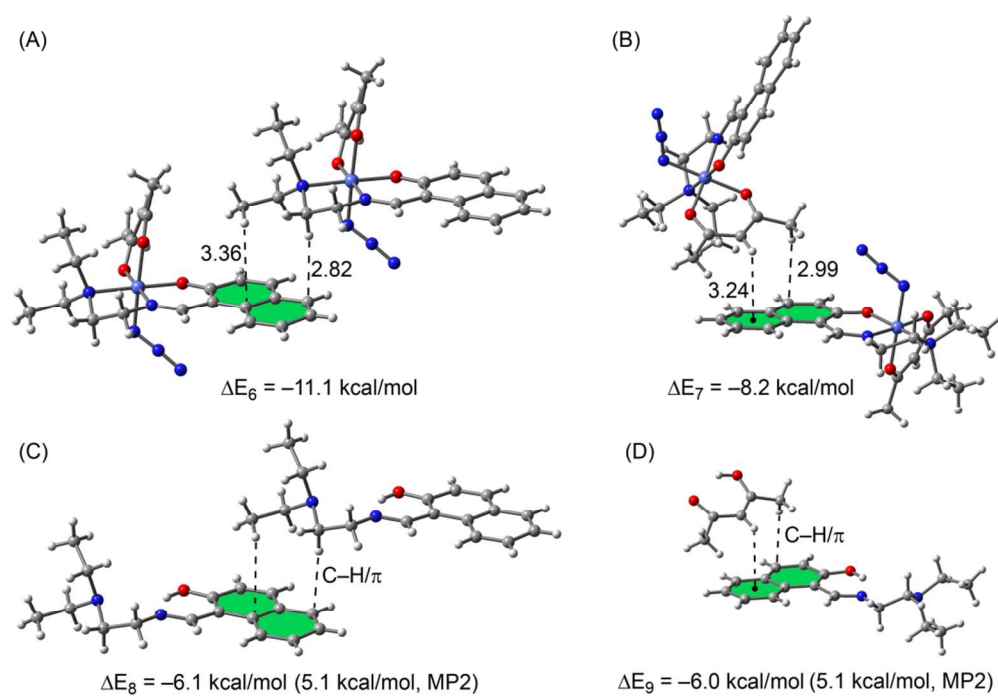


Figure 6: Theoretical models based of the X-ray structure of complex **2** used to evaluate the C–H/ π interactions. Distances are in Å.

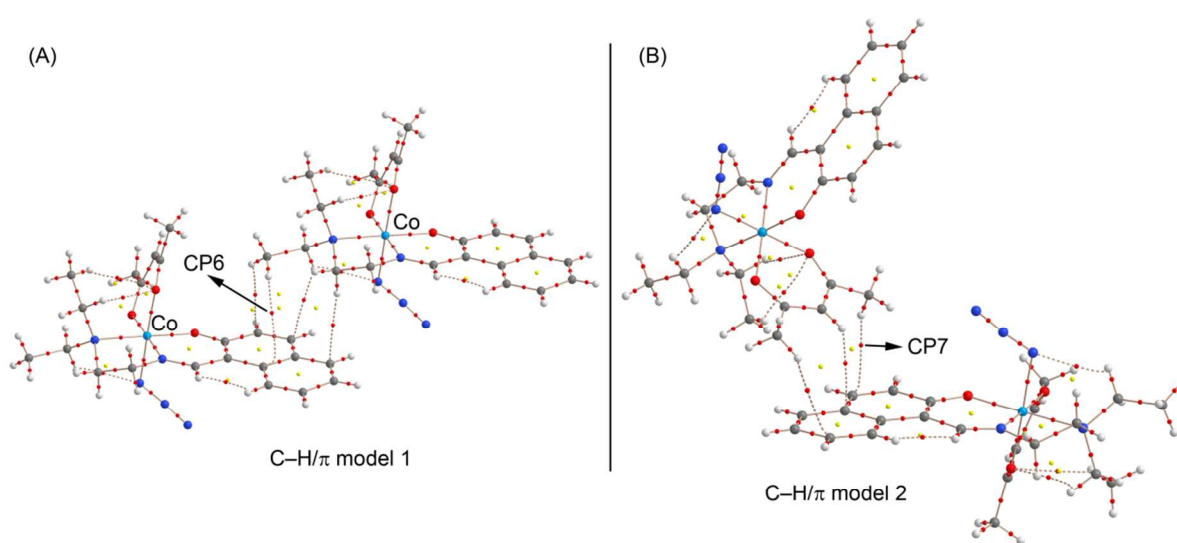


Figure 7: Distribution of bond and ring critical points (red and yellow spheres, respectively) and bond paths in two dimers of complex **2**.

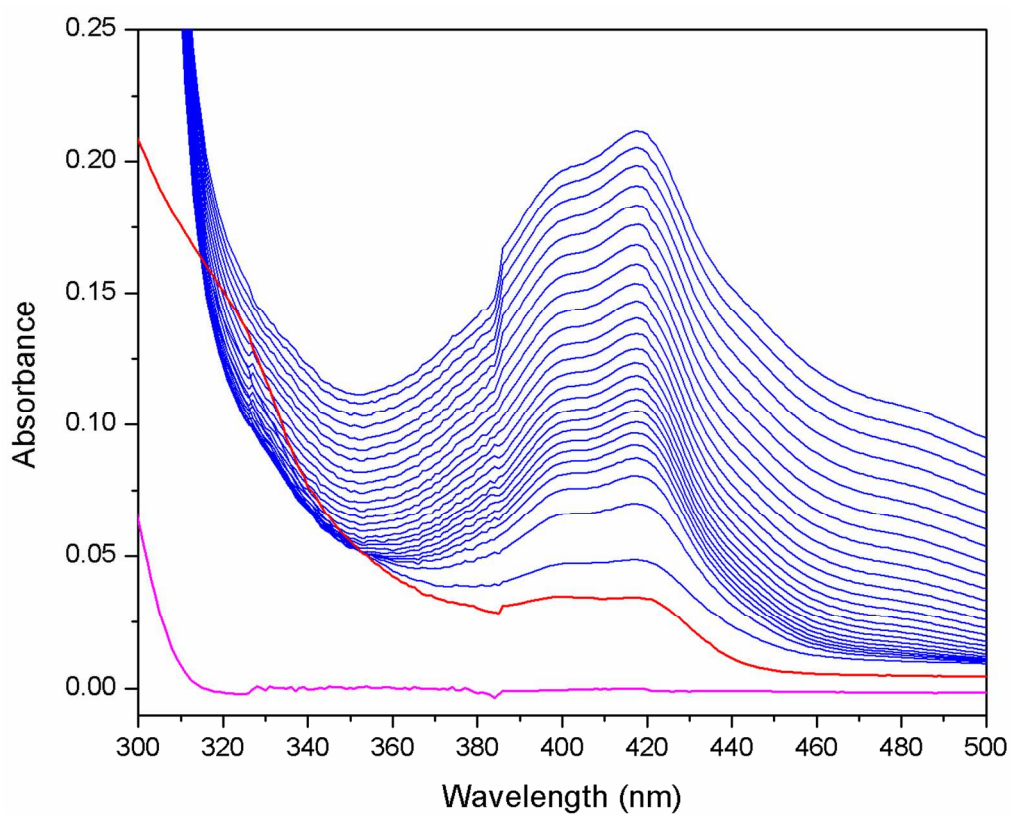


Figure 8: The spectral profile showing the growth of 2-aminophenoxazine-3-one at 433 nm upon addition of 10^{-3} M *o*-aminophenol to a solution containing complex **2** (1×10^{-5} M) in methanol. The spectra were recorded over a period of 2 h under aerobic conditions at room temperature.

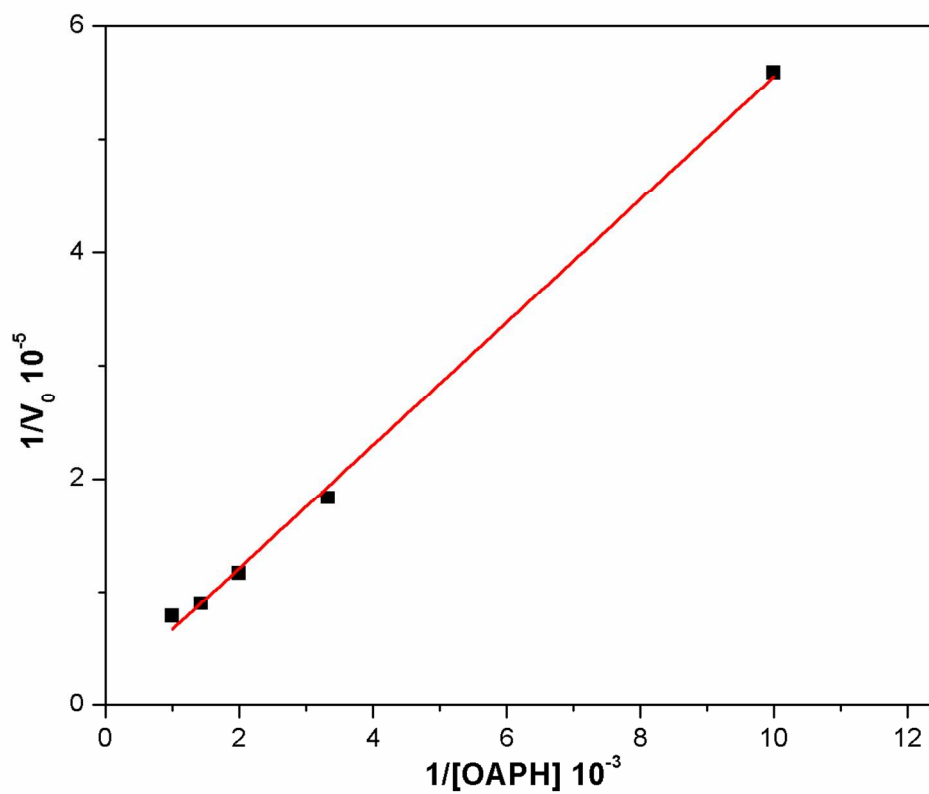


Figure 9: Linear Lineweaver–Burk plots for the oxidation of o-aminophenol catalyzed by complex **2**. Symbols and solid lines represent experimental and simulated profiles, respectively.

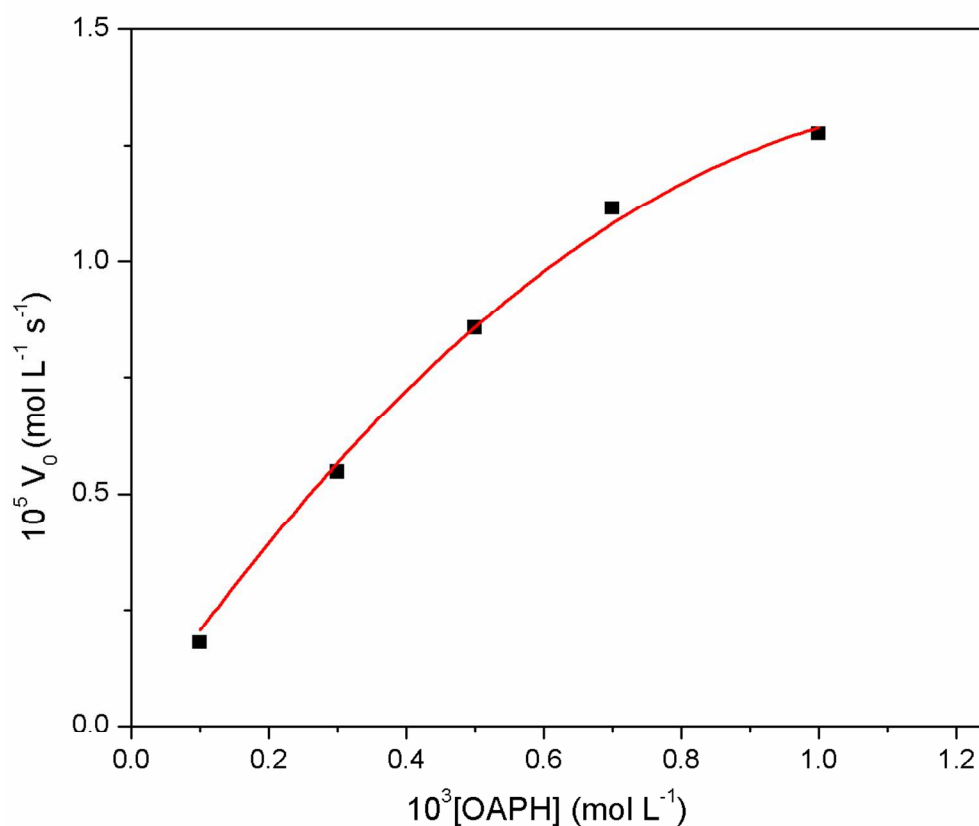


Figure 10: Initial rate versus substrate concentration plot for the oxidation of o-aminophenol in dioxygen-saturated methanol catalyzed by the complexes at room temperature. Symbols and solid lines represent the experimental and simulated profiles, respectively

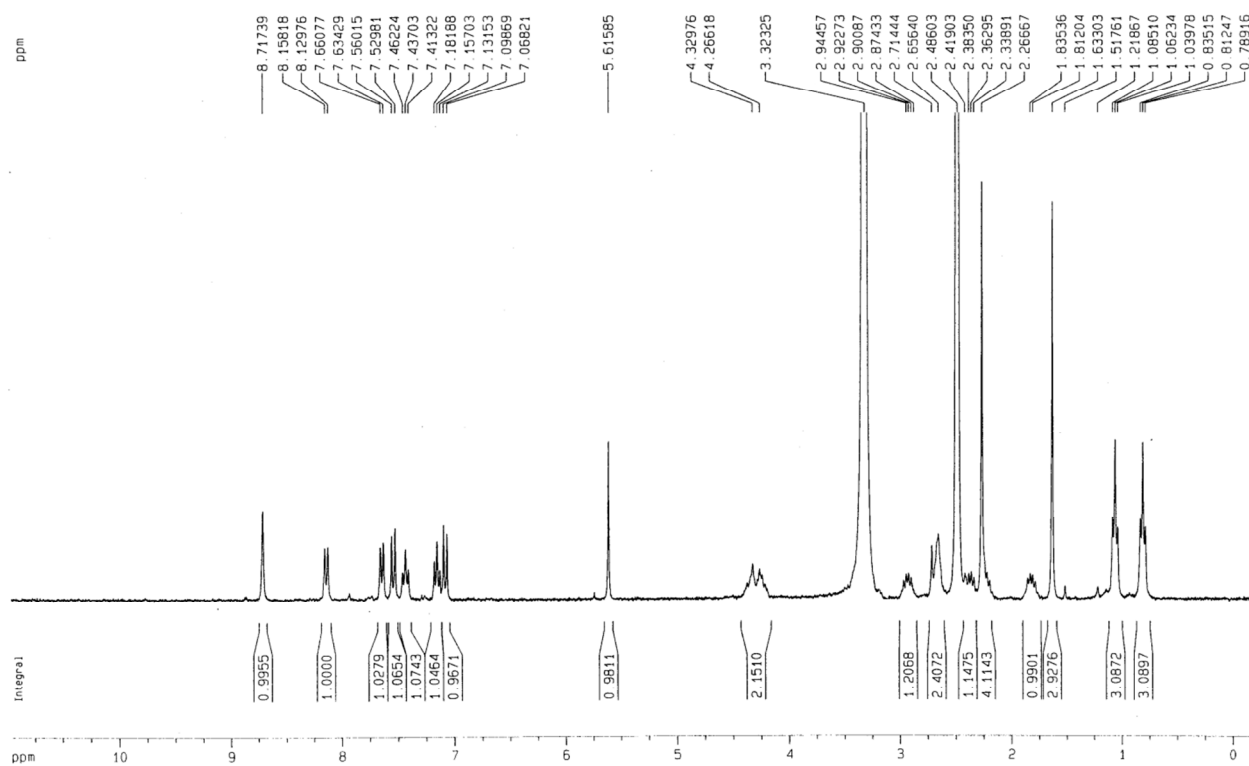


Figure 11: ^1H NMR spectrum of complex 2.

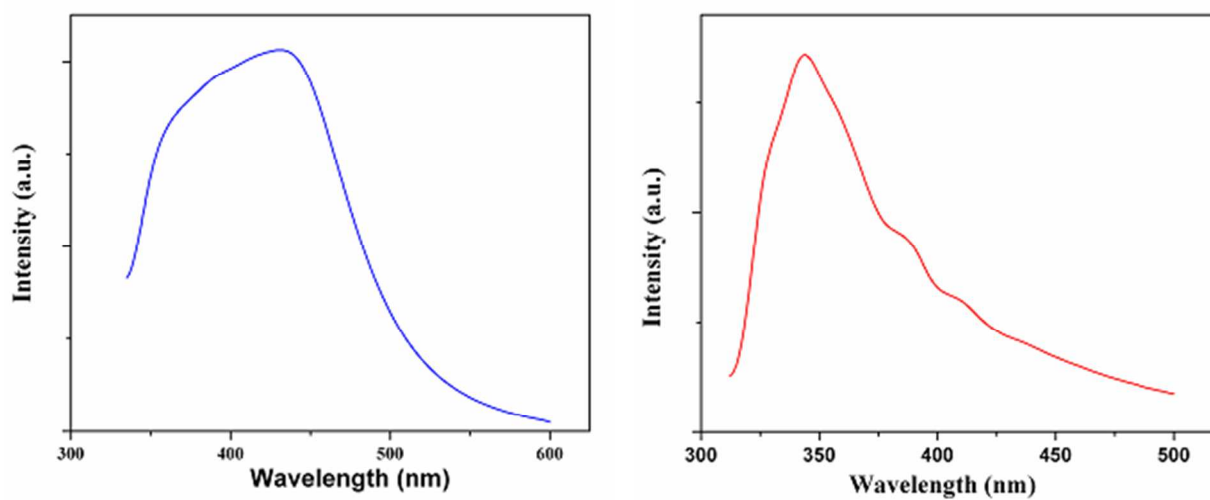


Figure 12: Photoluminescence spectra of complexes **1** (left) and **2** (right).

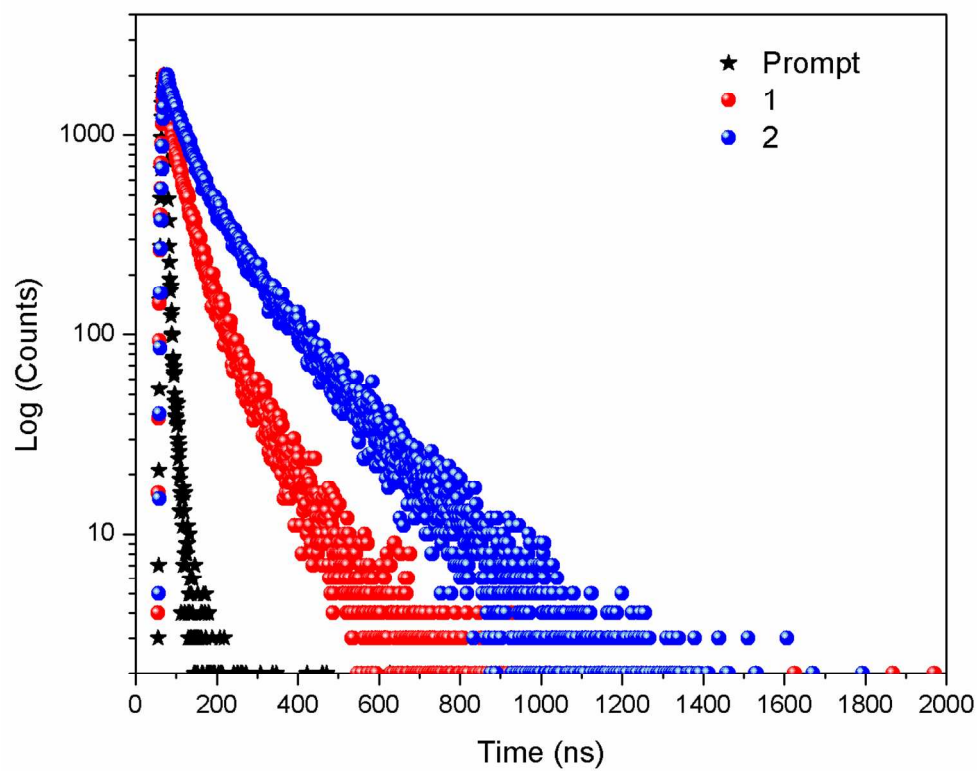


Figure 13: Time resolved photoluminescence decay profile of complexes **1** and **2** respectively.